Numerical Analysis of Electromagnetic Scattering by Electrically Large Objects Using Spatial Decomposition Technique

Korada R. Umashankar, *Senior Member, IEEE,* Sainath Nimmagadda, *Student Member, IEEE,* and Allen Taflove, *Fellow, IEEE*

Abstract—**The boundary value integral equation and method of moments numerical technique is widely utilized for the study of electromagnetic scattering by arbitrary shaped conducting and penetrable objects. Even though this direct approach is elegant as far as its application to analyze electrically large object is concerned, it inherently suffers from a wide range of computational difficulties. The method of moments system matrix is, in general, full and dense, requiring impractical demand on computer resources. In addition to operational numerical errors and ill-conditioning involved in the solution of large scale matrix equation, the direct numerical technique bears progressive degradation of accuracy of the near-field solution as the size of the system matrix increases. The apparent computational difficulties with the direct integral equation and method of moments has prompted an alternative numerical solution procedure based on the spatial decomposition technique. Using rigorous electromagnetic equivalence, the spatial decomposition technique virtually divides an electrically large object into a multiplicity of subzones. It permits the maximum size of the method of moments system matrix that need be inverted to be strictly limited, regardless of the electrical size of the large scattering object being modeled. The requirement on the computer resources is of order (N), where N is the number of spatial subzones and each subzone is electrically small spanning in the order of a few wavelengths. Numerical examples are reported along with comparative data and relative error estimation to expose applicability and limitation of the spatial decomposition technique for the two-dimensional scattering study of electrically large conducting and dielectric objects.**

I. Introduction

THE frequency domain analysis of electromagnetic scattering, penetration and interaction by arbitrary shaped conducting and dielectric objects can be conveniently formulated using the boundary value integro-differential equations. The boundary value equations, such as the electric field, the magnetic field and the combined field integral equations [1]–[3] have been extensively utilized to model various electromagnetic interactions associated with arbitrary shaped two and three dimensional objects. Generally, the near surface electric and magnetic fields or the corresponding equivalent magnetic and electric current distributions are treated as unknowns in the integral equations, and are solved by applying straight forward method of moments numerical technique [3]–[6]. Invariably, the numerical technique based on the method of moments converts the operator type of linear integral equation into an equivalent matrix equation by expanding the unknown current distributions in terms of a linearly independent set of expansion functions and testing the integral equation by a suitable set of weighting functions. This direct technique appears to be an elegant means for modeling and analyzing electromagnetic scattering and interaction by both canonical and arbitrary shaped conducting and dielectric objects. In fact, a large class of both two- and three-dimensional problems has been studied and reported extensively in the literature [3], [6]–[9]. However, there are key limitations and relative error estimations which render the direct integral equation and method moments technique unattractive beyond low and resonant frequencies.

The direct integral equation and method of moments technique generate a system of linear equations having dense, complex valued, full coefficient matrices. For a conventional matrix approach, the required computer storage is of the order $O(P^2) + C_pP$ where P is the number of surface patches and C_p is a constant which depends upon the scatterer geometry and desired display of the numerical solution. Similarly, the execution time is of the order of $O(P^2) + C_qP$ to $O(P^3) + C_rP$, where C_q and C_r are constants which depend upon numerical model adapted to generate the system matrix, and further, solve for the unknown surface currents. With a spatial resolution requirement in the order of $\lambda/5$–$\lambda/10$ to avoid aliasing of vital near-field magnitude and phase informa-

Manuscript received July 31, 1990; revised March 25, 1992. This work was supported in part by National Science Foundation Grant ASC-8811273 and by Office of Naval Research Grant N00014-88-K-0475.

K. R. Umashankar and S. Nimmagadda are with the Department of Electrical Engineering and Computer Science, University of Illinois, Chicago, IL 60680.

A. Taflove is with the Department of Electrical Engineering and Computer Science, McCormick School of Engineering, Northwestern University, Evanston, IL 60208.

IEEE Log Number 9201665.

tion implies that arbitrary three-dimensional structures spanning more than 5λ would exhaust most existing and planned mainframe computer resources [7], [10]. The dimensionally large computer resource requirement has, in fact, served to place such a "cap" on problem applications.

The large system matrix (of electrically large object) generated by the direct integral equation and method of moments numerical technique tends to become highly ill-conditioned. This potentially degrades the accuracy of the computed results [11]. The accuracy of the numerical solution may also be due to floating point word-length used in the computer and numerical procedure used for computing individual elements and inversion of the system matrix. Accumulating errors of these types can be troublesome, especially when hundreds of millions of matrix elements/floating point operations are involved in one modeling problem.

The computational difficulties with the direct integral equation and method of moments solution technique have prompted a number of alternative approaches, such as combining the method of moments and a high frequency technique to obtain a hybrid formulation [12], [13] and also its related iterative variations [14], [15]. In addition, iterative matrix solution methods including conjugate gradient, spectral iterative approaches [16], [17] have been investigated as tools to study electrically large scattering problems. It is not yet clear that the hybrid and iterative approaches proposed to date for electrically large objects possess the broad applicability and excellent accuracy that the full matrix method of moments approach evidences for the case of electrically small objects.

This paper presents preliminary findings of a novel methodology, which has been reported recently [3], [18], [19], [26], specifically referred to as the *spatial decomposition* technique (SDT) for the integral equation and method of moments that shows promise in significantly reducing both the dimensionality and ill-conditioning of the computational burden. In fact, the spatial decomposition permits the maximum size of the method of moments system matrix that need be inverted to be strictly limited, regardless of the electrical size of the electromagnetic scattering target being modeled. Using rigorous electromagnetic equivalences [20], the spatial decomposition technique allows one to divide an electrically large arbitrary shaped material object into a multiplicity of subzones. The individual subzones, in fact, are separated by virtual surfaces across which cancelling tangential electric and magnetic virtual currents are postulated. The subzones are defined as distinct scattering targets having fully enclosing surfaces with additional unknown virtual electric and magnetic currents introduced as needed to define the interfaces. The electromagnetic field boundary conditions are well preserved by simulating across the interface separating two subzones by requiring that the tangential virtual currents on one side of the interface must be equal but opposite to the tangential virtual currents on the other side. By sequentially implementing the integral equation and method of moments solution for each subzone, effectively "scanning" the original target subzone by subzone, a rapidly convergent iterative process is established.

This paper reports a preliminary study of the spatial decomposition technique to analyze electromagnetic scattering by arbitrary shaped electrically large two-dimensional perfectly conducting and dielectric scatterers. Numerical results of the near surface currents and radar cross section along with comparative validation data and relative error estimation based on matrix condition number [21], [22] are reported in this paper to expose applicability and limitation of the SDT for electromagnetic scattering by an electrically large perfectly conducting thin strip scatterer, perfectly conducting rectangular and wedge type scatterers and homogeneous dielectric rectangular scatterer.

II. Spatial Decomposition Technique

Fig. 1 illustrates an arbitrary shaped two-dimensional isotropic homogeneous dielectric scattering object. It is excited externally by a transverse magnetic (TM) polarized plane wave propagating in a direction normal to the z-coordinate axis. As shown in Fig. 1, axially directed equivalent electric currents $J_z(\bar{\rho}')$ and transverse directed equivalent magnetic currents $M_\tau(\bar{\rho}')$ reside on a virtual boundary conforming to the physical surface of dielectric scatterer. This scattering object, in fact, is appropriate for formulating a set of coupled combined field integral equations (CFIE) by invoking the electromagnetic equivalence principle [2], [7], [20] and by treating the two surface electric and magnetic currents as initially unknown distributions. Further, the method of moments numerical technique can be implemented (for the scatterer taken as a whole) to solve for the two unknown surface currents as discussed in [3], [6], [9]. There exist only the following components of electric and magnetic field distributions:

$E_z(\rho, \phi)\hat{\mathbf{z}}$ total axial component of electric field distribution

$H_\nu(\rho, \phi)\hat{\nu}$ total normal component of magnetic field distribution

$H_\tau(\rho, \phi)\hat{\mathbf{s}}$ total tangential component of magnetic field distribution.

Referring to Fig. 1,

$$\bar{J}_{eq}(\bar{\rho}') = \hat{z}' J_z(\bar{\rho}') \tag{1a}$$

$$= \hat{\nu}' \times \hat{s}' H_\tau(\rho', \phi'), \qquad \bar{\boldsymbol{\rho}}' \text{ on } C \tag{1b}$$

$$\bar{M}_{eq}(\bar{\rho}') = \hat{s}' M_\tau(\bar{\rho}') \tag{2a}$$

$$= -\hat{\nu}' \times \hat{z}' E_z(\rho', \phi'), \qquad \bar{\boldsymbol{\rho}}' \text{ on } C. \tag{2b}$$

For the TM normal excitation, based on the above components of unknown electric and magnetic current distributions, the z-component of scattered electric field

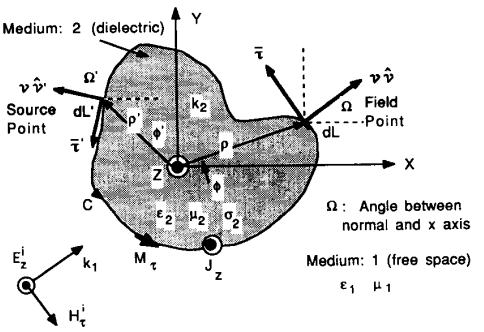

Fig. 1. Geometry of homogeneous, lossy, dielectric scatterer.

and τ-component of scattered magnetic field are obtained by

$$\pm E^s_{mz}(\bar{\rho}) = -\hat{z}\cdot j\omega \bar{A}_m(\bar{\rho},\omega) - \hat{z}\cdot\nabla_\tau \times \frac{1}{\epsilon_m}\bar{F}_m(\bar{\rho},\omega) \tag{3a}$$

$$\pm H^s_{m\tau}(\bar{\rho}) = -\hat{\tau}\cdot j\omega \bar{F}_m(\bar{\rho},\omega) - \frac{\partial}{\partial s}\Psi_m(\bar{\rho},\omega) + \hat{s}\cdot\nabla_\tau \times \frac{1}{\mu_m}\bar{A}_m(\bar{\rho},\omega) \tag{3b}$$

where on the left-hand side, the positive sign is selected for the region ($m = 1$) outside the dielectric scatterer with $\bar{\rho}$ on or outside the boundary contour C, and the negative sign is selected for the region ($m = 2$) inside the dielectric scatterer with $\bar{\rho}$ on or inside the boundary contour C. The vector and scalar potential integrals in (3a) and (3b) are given

$$\bar{A}_m(\bar{\rho}) = \frac{\mu_m}{4j}\int_C \hat{z}' J_z(\bar{\rho}') H_0^{(2)}\left(k_m|\bar{\rho}-\bar{\rho}'|\right) dL(\bar{\rho}') \tag{4a}$$

$$\bar{F}_m(\bar{\rho}) = \frac{\epsilon_m}{4j}\int_C \hat{s}' M_\tau(\bar{\rho}') H_0^{(2)}\left(k_m|\bar{\rho}-\bar{\rho}'|\right) dL(\bar{\rho}') \tag{4b}$$

$$\Psi_m(\bar{\rho}) = \frac{1}{4\omega\mu_m}\int_C [\nabla'_\tau\cdot\hat{s}' M_\tau(\bar{\rho}')] \cdot H_0^{(2)}\left(k_m|\bar{\rho}-\bar{\rho}'|\right) dL(\bar{\rho}'),$$

for $m = 1$, $\bar{\rho}$ on or outside C (free space medium)

for $m = 2$, $\bar{\rho}$ on or inside C (dielectric medium) (4c)

and

$H_0^{(2)}\left(k_m|\bar{\rho}-\bar{\rho}'|\right)$ Green's function for the two-dimensional case—Hankel function of zero-order and second kind

k_m: propagation constant for $m = 1$ and $m = 2$ regions $= \omega\sqrt{\mu_m\epsilon_m}$. (4d)

The complete derivation of the coupled combined field integral equations can be found in [2], [3], [7], [6], and [9] by invoking the electromagnetic equivalences for regions 1 and 2, and the boundary conditions that the tangential components of total electric and magnetic fields are continuous across the boundary C. Only a summary of the relevant CFIE expressions which are useful for development of the spatial decomposition technique are given below

$$E^i_z(\bar{\rho}) = \sum_{m=1}^{2}\mathscr{L}_m^{JJ}[J_z(\bar{\rho}')] + \sum_{m=1}^{2}\mathscr{L}_m^{JM}[M_\tau(\bar{\rho}')], \qquad \bar{\rho}\text{ on } C \tag{5a}$$

$$H^i_\tau(\bar{\rho}) = \sum_{m=1}^{2}\mathscr{L}_m^{MJ}[J_z(\bar{\rho}')] + \sum_{m=1}^{2}\mathscr{L}_m^{MM}[M_\tau(\bar{\rho}')], \qquad \bar{\rho}\text{ on } C \tag{5b}$$

where the CFIE partial integral operators [3], [6], [9] for the two-dimensional case are

$$\mathscr{L}_m^{JJ} = \int_C\left[\frac{\omega\mu_m}{4}H_0^{(2)}(k_m R)\right]dL' \tag{6a}$$

$$\mathscr{L}_m^{JM} = \oint_C\left\{\frac{x-x'}{R}\cos\Omega' + \frac{y-y'}{R}\sin\Omega'\right\}\cdot\left[\frac{k_m}{4j}H_0^{(2)'}(k_m R)\right]dL' \tag{6b}$$

$$\mathscr{L}_m^{MJ} = \oint_C\left\{\frac{x-x'}{R}\cos\Omega + \frac{y-y'}{R}\sin\Omega\right\}\cdot\left[\frac{k_m}{4j}H_0^{(2)'}(k_m R)\right]dL' \tag{6c}$$

$$\mathscr{L}_m^{MM} = \int_C\cos(\Omega-\Omega')\left[\frac{\omega\epsilon_m}{4}H_0^{(2)}(k_m R)\right]dL' + \frac{\partial}{\partial s}\int_C dL'\left[\frac{1}{4\omega\mu_m}H_0^{(2)}(k_m R)\right]\frac{\partial}{\partial s'}, \qquad m = 1,2. \tag{6d}$$

In (5a) and (5b), E^i_z represents the TM polarized axial component of the incident plane wave electric field excitation and H^i_τ represents corresponding transverse component of the incident magnetic field excitation. In the case of direct method of moments solution [4]–[7], the axial electrical current J_z and the transverse magnetic current M_τ distributions are expanded in terms of suitable expansion functions, such as, staggered pulse expansion functions discussed in [7]. Further, the coupled CFIE expressions (5a) and (5b) are tested on both sides by the weighting functions chosen to be same as the expansion functions in order to reduce the coupled set of integral equations to their equivalent partitioned matrix equation. Based on the direct method of moments numerical solution, extensive numerical data for the near surface current distributions and the radar cross section results are reported in the literature [5]–[9] both for the electrically

small and the resonant size conducting and dielectric scattering objects. As the electrical size of the scatterer increases, this direct solution technique puts impractical demand on the computer resources, in addition to various unsettled numerical accuracy and ill-conditioning problems of the large system matrix associated with the electrically very large object.

In order to circumvent high demand on the computer resources and also reduce numerical difficulties, the formulation of the boundary value problem is modified still retaining all the physics of electromagnetic scattering and interaction as depicted schematically in Figs. 2(a) and 2(b). Fig. 2(a) represents a rectangular homogeneous dielectric scatterer geometry with unknown surface electric and magnetic current distributions on a virtual boundary. An identical geometry is repeated in Fig. 2(b), but the virtual boundary contour is modified to define (in this case) two distinct spatial subzones. A key point to note is that at the virtual interface separating the two subzones, the tangential virtual currents on one side of the interface must be equal, but opposite to the tangential virtual currents on the other side of the interface. In fact, the scatterer can be divided into an arbitrary number of N distinct spatial subzones in this manner (in Fig. 2(b), $N = 2$). Now, the usual combined field integral equation and method of moments technique is used to compute the electric and magnetic currents along the enclosing surface of one subzone. In effect, the subzone is treated as a distinct scatterer. It should be noted that a part of the subzone's surface is the virtual interface separating it from the adjacent subzone. The excitation for this subzone consists of the original incident plane wave and additional excitation due to the electric and magnetic currents residing on the surfaces on the remaining spatial subzones and radiating into the free space. Initially, the additional excitation due to the currents on the remaining spatial subzones is not known. But, these can be conveniently approximated to a zeroth-order using either the physical optics (PO) [23] or possibly a first-order better approximation based on the on-surface radiation condition (OSRC) theory [24], [25]. Hence, for subzone 1, the CFIE takes the form

$$F_z^i(\bar{\rho}) = \sum_{m=1}^{2} \mathscr{L}_m^{JJ}[J_{z1}(\bar{\rho}')] + \sum_{m=1}^{2} \mathscr{L}_m^{JM}[M_{\tau 1}(\bar{\rho}')] \quad (7a)$$

$$G_\tau^i(\bar{\rho}) = \sum_{m=1}^{2} \mathscr{L}_m^{MJ}[J_{z1}(\bar{\rho}')] + \sum_{m=1}^{2} \mathscr{L}_m^{MM}[M_{\tau 1}(\bar{\rho}')], \quad \text{for subzone 1, } \bar{\rho} \text{ on } C_1 \quad (7b)$$

$J_{z1}(\bar{\rho}')$ unknown electric current distribution for the subzone 1

$M_{\tau 1}(\bar{\rho}')$ unknown magnetic current distribution for the subzone 1

where the boundary contour C_1 encloses completely the spatial subzone 1. The total excitation for the spatial subzone 1 is given by plane wave excitation and additional

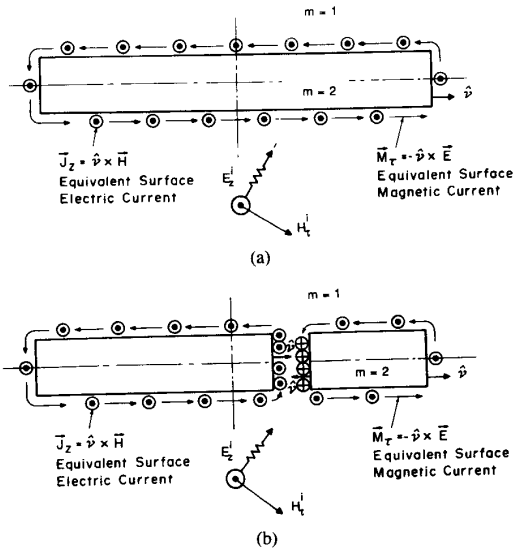

Fig. 2. (a) Distribution of equivalent electric and magnetic currents on a virtual surface. (b) Distribution of equivalent electric and magnetic currents on a modified virtual surface for the spatial decomposition technique.

excitation due to the remaining spatial subzones, $n = 2, 3, 4, \cdots, N$

$$F_z^i(\bar{\rho}) = E_z^i(\bar{\rho}) - \sum_{n=2}^{N} \mathscr{L}_1^{JJ}[J_{zn}(\bar{\rho}_n')] - \sum_{n=2}^{N} \mathscr{L}_1^{JM}[M_{\tau n}(\bar{\rho}_n')] \quad (8a)$$

$$G_\tau^i(\bar{\rho}) = H_\tau^i(\bar{\rho}) - \sum_{n=2}^{N} \mathscr{L}_1^{MJ}[J_{zn}(\bar{\rho}_n')] - \sum_{n=2}^{N} \mathscr{L}_1^{MM}[M_{\tau n}(\bar{\rho}_n')], \quad \text{for subzone 1, and } \bar{\rho}_n' \text{ on } n\text{th subzone boundary } C_n. \quad (8b)$$

The analysis is now shifted to the next adjacent subzone. The excitation for this subzone consists of the original plane wave and additional excitation due to the currents on the surfaces of the remaining subzones, including the updated currents on the first subzone. In this manner, the step-by-step analysis approach can be sequentially implemented for rest of the subzones, effectively scanning the original scatterer subzone by subzone, always using the incident plane wave and the latest surface currents as the excitation for the subzone of interest. This iterative process appears to differ from any yet proposed in that: 1) subzones are used rather than the complete structure at a time, and 2) the subzones are not completely related to individual blocks of the original full matrix problem; rather, the subzones are defined as distinct targets having fully enclosing boundary surfaces with additional virtual electric and magnetic current unknowns (still maintaining the boundary conditions) introduced as needed to define the virtual interface consistently between the subzones.

Thus, the SDT provides means to implement the existing integral equation and method of moments technique with a computer memory and execution time requirement of $O(N)$, where N is the number of spatial subzones. Since each subzone is electrically small, spanning few wavelengths either in the two- or three-dimensional scattering problems, it is expected that conditioning of the method of moments system matrix resulting for each subzone is acceptable for numerical processing with limited demand on computer resources. In the following, several scattering case studies are presented along with relative error estimation based on the matrix condition number [21], [22] to expose preliminary studies of the SDT to analyze electromagnetic scattering by two-dimensional perfectly conducting and dielectric scatterers. Numerical results of the surface electric current and radar cross section data along with comparison based on the direct Gauss–Seidel algorithm are reported in this paper for the perfectly conducting thin strip scatterer, perfectly conducting rectangular and wedge type scatterers and homogeneous dielectric rectangular scatterer.

III. Perfectly Conducting Scatterer—TM Case

In order to illustrate the spatial decomposition technique, the electromagnetic scattering by a perfectly conducting thin strip and a rectangular scatterer are considered. Referring to Fig. 2(a), the conductivity of the scatterer is assumed to be infinite in a limit, and the thickness of the rectangular geometry is reduced to zero. For the case of TM normal excitation, there exists only an axially directed electric current along the length of thin strip scatterer given by the difference between the top and bottom current distributions. Referring to (5a) and (6a), the electric field integral equation (EFIE) for the two-dimensional perfectly conducting case is given by [1]–[3]

$$E_z^i(\bar{\rho}) = \mathscr{L}_1^{JJ}[J_z(\bar{\rho}')], \qquad \bar{\rho} \text{ on thin strip} \tag{9a}$$

where for the TM excitation

$$\mathscr{L}_1^{JJ} = \int_C \left[\frac{\omega\mu_1}{4} H_0^{(2)}(k_1 R)\right] dL' \tag{9b}$$

and the incident plane wave electric field can be written as

$$E_z^i(\rho, \phi) = E_0 e^{-jk_1\rho\cos(\phi - \phi^i)} \tag{9c}$$

ϕ^i incident angle of the TM polarized plane wave excitation.

The distribution of the electric current on the thin strip scatterer can be directly obtained by applying the method of moments numerical technique [4] by using a pulse expansion set for representing the unknown electric current distribution, and also testing the EFIE expression (9a) by the same pulses. Fig. 3(a) shows a plot of the magnitude of electric current on a thin strip scatterer of total length, $L = 25\lambda$, excited at an angle of incidence $\phi^i = 90°$. This result is obtained using a full matrix of size (250×250) with a current resolution of 10 pulse samples per wavelength. In order to apply the spatial decomposition technique, the thin strip scatterer is divided, for example, into five subzones, $N = 5$. Maintaining the same current resolution of 10 samples per wavelength, the matrix size is now only (50×50) for each subzone modeling. Referring to (7a) and (8a), the EFIE for the first subzone has the form

$$E_z^i(\bar{\rho}) - \sum_{n=2}^{5} \mathscr{L}_1^{JJ}[J_{zn}(\bar{\rho}_n')] = \mathscr{L}_1^{JJ}[J_{z1}(\bar{\rho}')], \qquad \bar{\rho} \text{ on subzone 1.} \tag{10}$$

On the left-hand side of the SDT expression (10), the total excitation for the spatial subzone 1 is given by the plane wave excitation and additional excitation due to the electric currents on remaining spatial subzones, $n = 2$, 3, 4 and 5. But, the distributions of the electric current on the remaining subzones, $n = 2$, 3, 4 and 5, are not known initially. However, they can be obtained approximately based on either the PO [23] or the OSRC approach [24], [25]. An approximate distribution of the electric current on a perfectly conducting scatterer is obtained using the normal derivative of the total electric field, and for subzones $n = 2$, 3, 4 and 5 is given by

$$J_{zn}(\bar{\rho}') = \frac{-j}{\eta_1 k_1}\left[\frac{\partial E_z^s(\bar{\rho}')}{\partial \nu'} + \frac{\partial E_z^i(\bar{\rho}')}{\partial \nu'}\right] \tag{11}$$

where η_1 is the intrinsic impedance of the free space medium. Using the second-order OSRC boundary operator [22], an approximate relationship for the normal derivative of axially directed scattered electric field on the perfectly conducting convex scatterer can be obtained as

$$\frac{\partial E_z^s(\bar{\rho}')}{\partial \nu'} = \left[\frac{\xi(s')}{2} + jk_1 + \frac{j\xi^2(s')}{8[k_1 - j\xi(s')]}\right] E_z^i(\bar{\rho}) + \frac{j}{2[k_1 - j\xi(s')]} \frac{\partial^2 E_z^i(\bar{\rho}')}{\partial s'^2}. \tag{12a}$$

$\xi(s')$ curvature of an osculating circle drawn tangential to the boundary contour

s' tangential coordinate variable along the boundary contour, and

$$\frac{\partial^2 E_z^i(\bar{\rho}')}{\partial s'^2} = -K^2[\sin^2\Omega'\cos^2\phi^i + \cos^2\Omega'\sin^2\phi^i - 2\sin\Omega'\cos\Omega'\cos\phi^i\sin\phi^i]E_z^i(\bar{\rho}'). \tag{12b}$$

With the normal broadside excitation, $\phi^i = 90°$, the above OSRC expression yields an initial current distribution, which is a flat current, with no current singularities at the thin strip scatterer ends. In fact, the goal of the SDT is to sequentially update this initial current for each subzone. The analysis is now shifted to the adjacent subzone $n = 2$. The excitation for this subzone 2 consists of the original plane wave plus additional excitation due

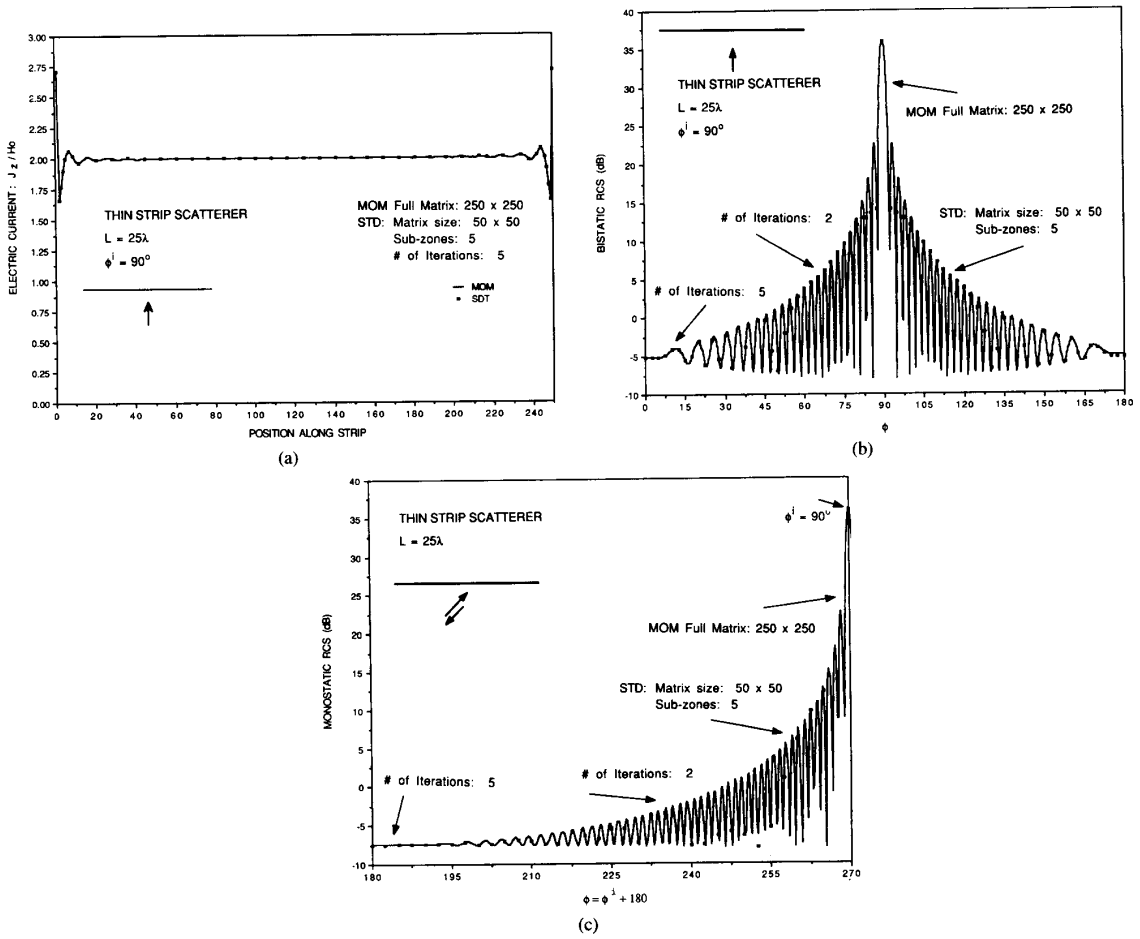

Fig. 3. (a) Distribution of the equivalent electric current on the thin strip scatterer—TM normal excitation. (b) Bistatic radar cross section of the thin strip scatterer—TM normal excitation. (c) Monostatic radar cross section of the thin strip scatterer—TM normal excitation.

to the approximate currents on the surface of the remaining subzones, $n = 3$, 4 and 5 including the updated current along the first subzone. This step-by-step analysis approach is sequentially implemented in an iterative sweep for each subzone from one end of the scatterer to the other end. Once the first sweep is completed, a first-order approximate distribution of the electric current on the thin strip scatterer is numerically simulated. It is noted here that no additional boundary conditions are enforced in the application of SDT. Better approximation of the distribution of magnitude and phase of the electric current on the thin strip scatterer can be obtained by more iterative sweeps. In Fig. 3(a) is shown the distribution of the magnitude of electric current calculated based on the SDT (with five spatial subzones, $N = 5$) on the thin strip scatterer excited with an angle of incidence $\phi^i = 90°$. The results shown are obtained for five sweeps with less than 1% error in the region separating two adjacent subzones. It should be noted that the electric currents are valid only for the specified angle of incidence and the SDT iterative process is to be repeated if the numerical data for other angles of incidence is required. The distribution of the electric current can now be utilized for calculating either the near electric and magnetic field distributions or the bistatic radar cross-section data. In fact, the number of successive iterative sweeps is determined based on the degree of convergence required of the electric current or the radar cross-section data. The far-field distribution and the radar cross-section data can be derived using (3a), (4a), and (9b) with the two-dimensional Green's function term replaced with its large argument approximation. Fig. 3(b) shows a plot of the bistatic radar cross section obtained using SDT compared with the direct method of moments (MM) solution. In the angular range of $\phi = 30°$ to 150°, the bistatic radar cross section converges in two sweeps with less than 1% error, but for the grazing angles more sweeps are required, and for the results shown five sweeps are utilized. Fig. 3(c) shows a plot of the monostatic radar cross section obtained using SDT compared with respect to the direct (MM) solution.

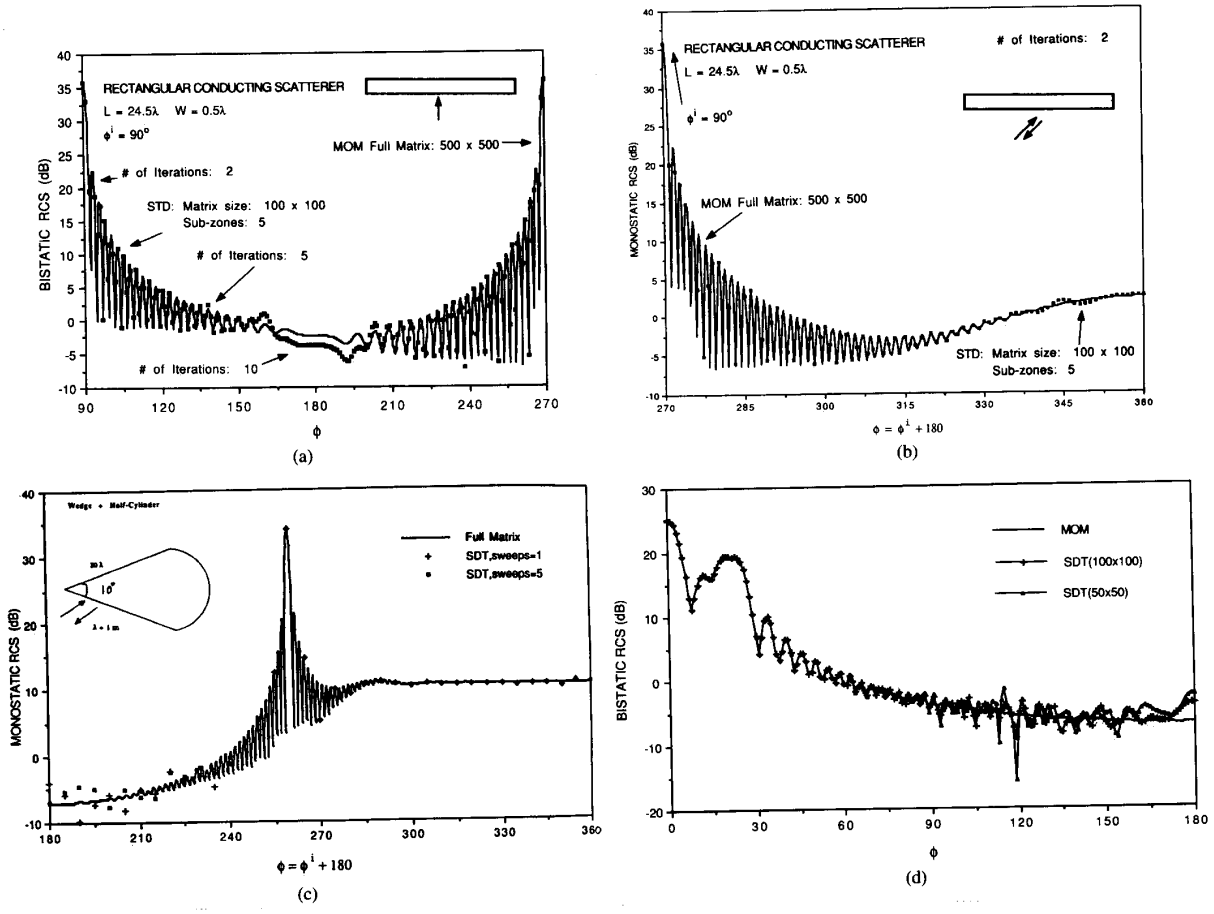

Fig. 4. (a) Bistatic radar cross section of the rectangular conducting scatterer—TM normal excitation. (b) Monostatic radar cross section of the rectangular conducting scatterer—TM normal excitation. (c) Monostatic radar cross section of the wedge with half-cylinder—TM excitation. (d) Bistatic radar cross section of the wedge with half-cylinder—TM excitation.

In fact, numerical studies indicate smaller subzone sizes [18] can be adapted with even lower computer resources, but require more iterative sweeps for the same degree of convergence. Tables I, II, and III show computer resources required on a Sun 4.0 Workstation as a function of subzone size and number of iterative sweeps. The representative case of thin strip scatterer of total length $L = 10\lambda$ excited at an angle of incidence, $\phi^i = 90°$, is considered with a finer current resolution of 20 pulse samples per wavelength. The results reported here are based on a general unoptimized computer algorithm with Gauss–Seidel numerical inversion. The run times reported in the tables, in fact, are higher than many standard optimized algorithms [3], [7].

Similar convergence behavior is observed for other bistatic and monostatic angles. The above studies using SDT can be easily extended for the case of electromagnetic scattering by a perfectly conducting rectangular and wedge type scatterers. Fig. 4(a) shows a plot of bistatic radar cross section of a rectangular scatterer of total length $L = 24.5\lambda$ and width $W = 0.5\lambda$ which is excited at an angle of incidence $\phi^i = 90°$. This result is obtained using a full matrix of size (500 × 500) for the direct MM solution. Similar to the thin strip case discussed earlier, in

TABLE I
DIRECT MM SOLUTION

Full Matrix Size Total	Bistatic RCS in decibels Observation Angle, $\phi = 90°$	Run Time in Seconds
200	27.971437	205.2

TABLE II
SDT SOLUTION—VARIATION OF NUMBER OF SUBZONES (NUMBER OF SWEEPS = 1)

Subzone Matrix Size	Number of Subzones	Bistatic RCS in decibels Observation Angle, $\phi = 90°$	Run Time in Seconds
20	10	27.95345306	10.0
25	8	27.97183609	12.6
40	5	27.96068573	23.9
50	4	27.97832870	34.1
100	2	27.96839523	121.0

TABLE III
SDT SOLUTION—VARIATION OF NUMBER OF SWEEPS
(SUBZONE MATRIX SIZE = 50 AND NUMBER OF SUBZONES = 4)

Number of Sweeps	Bistatic RCS in decibels Observation angle, $\phi = 90°$	Run Time in Seconds
1	27.97832870	34.1 per sweep
2	27.97290012	
3	27.97251701	
4	27.97248459	
5	27.97203225	
6	27.97153854	
7	27.97137260	
8	27.97138977	
9	27.97143173	
10	27.97144699	

order to apply the spatial decomposition technique, the scatterer is divided into five subzones, $N = 5$, and the matrix size is chosen with the same uniform resolution for each subzone modeling. Fig. 4(a) also shows a plot of the bistatic radar cross section obtained using SDT compared with the direct MM solution. Both forward and back scattering data in the angular range $\phi = 90°$ to 120° converge with only two iterative sweeps, and for the angular range $\phi = 120°$ to 150° convergence is obtained with five sweeps with less than 1% error. However, for the grazing angles more sweeps are required, and for the bistatic results shown 10 sweeps are utilized. The monostatic data, on the other hand, converges rapidly with only two iterative sweeps. Fig. 4(b) shows a plot of the monostatic radar cross section obtained using SDT with two sweeps compared with the direct MM solution. The monostatic study has been extended even for the case of a conducting wedge type scatterer. Fig. 4(c) shows a plot of the monostatic radar cross section obtained for a two-dimensional finite length wedge with half-cylinder. Fig. 4(d) shows bistatic radar cross sections obtained using subzones of (100 × 100) and (50 × 50) matrix systems. TM normal excitation with $\phi^i = 0°$ is assumed to be incident on the tip of the wedge. In Figs. 4(c) and 4(d), the SDT numerical results are compared with the direct MM solution.

IV. ERROR ANALYSIS BASED ON MATRIX CONDITION NUMBER

It is evident that the SDT offers substantial savings in computer storage and time as compared to the direct integral equation and method of moments solution. From error analysis and estimation point of view, the SDT deals with only smaller matrices arising due to division of the large scatterer into multiplicity of subzones. The Gauss–Seidel inversion of matrices inevitably introduces round-off errors, the extent of which essentially depends on the sophistication of computing device and its word-length. In fact, round-off errors are fairly random in nature and do not cancel out in a given computation, but rather tend to accumulate if later calculations are based on the earlier ones. A detailed discussion concerning relative error analysis and estimation of the degree ill-conditioning associated with typical method of moments scattering problems is addressed in [21] and [22] using a qualitative figure, such as, the matrix condition number. A convenient measure of the condition of a matrix can be assessed in defining

$$\text{cond}([Z]) = \|Z\| \cdot \|Z^{-1}\| \tag{13a}$$

where considering the infinite norm, the maximum row sum of the matrix

$$\|Z\| = \|Z\|_\infty. \tag{13b}$$

In solving the matrix equation, the condition number of matrix represents an upper bound on the relative uncertainty in determining the electric current distribution. Just in the numerical inversion alone, the direct method requires arithmetic operations proportional to third power of the matrix size. But, in the SDT only very small matrices are dealt with proportional to electrical size of subzones. Fig. 5 shows variation of worst-case condition number with number of subzones for the strip and rectangle cases studies discussed above. Thus, the submatrices corresponding to the subzones are better conditioned than the large matrix of the direct method. The condition of the subzone matrix improves as it becomes smaller, however, this improvement cannot be extracted indefinitely in view of the stronger coupling and interaction with very small subzones.

V. PERFECTLY CONDUCTING SCATTERER—TE CASE

The preliminary study of the spatial decomposition technique is reported for the case of perfectly conducting thin strip scatterer with transverse electric (TE) excitation. For the case of TE normal excitation, there exists only a tangentially directed electric current along the boundary of scatterer. Referring to (5b) and (6d), and considering its dual representation for the induced electric current, the EFIE is given by [1]–[3]

$$E_\tau^i(\bar{\rho}) = \int_C \cos(\Omega - \Omega') J_\tau(\bar{\rho}') \left[\frac{\omega\mu_1}{4} H_0^{(2)}(k_1 R)\right] dL' + \frac{\partial}{\partial s} \int_C \frac{\partial}{\partial s'} J_\tau(\bar{\rho}') \left[\frac{1}{4\omega\epsilon_1} H_0^{(2)}(k_1 R)\right] dL', \quad \bar{\rho} \text{ on thin strip.} \tag{13}$$

Again, the distribution of the electric current on the thin strip scatterer can be directly obtained by using a pulse expansion set for representing the unknown electric current distribution, and also testing the EFIE expression (13) by the same pulses. Fig. 6(a) shows a plot of the magnitude of electric current on a thin strip scatterer of total length, $L = 25\lambda$, excited at an angle of incidence $\phi^i = 90°$. This result is obtained using a full matrix of size (250 × 250) with a current resolution of 10 pulse samples per wavelength. Similar to the TM case discussed earlier, in order to apply the spatial decomposition technique, the thin strip scatterer is divided into five subzones, $N = 5$. Providing the same resolution, the SDT matrix size is only

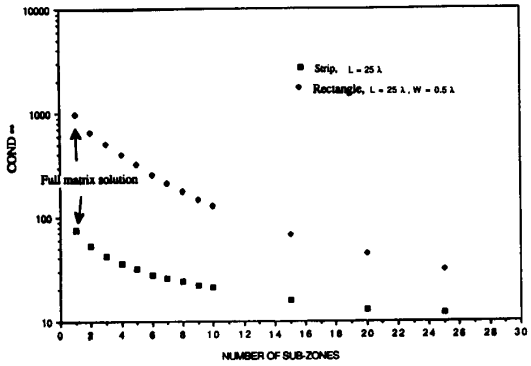

Fig. 5. Variation of worst-case condition number with number of subzones—strip and rectangular scatterers—TM excitation.

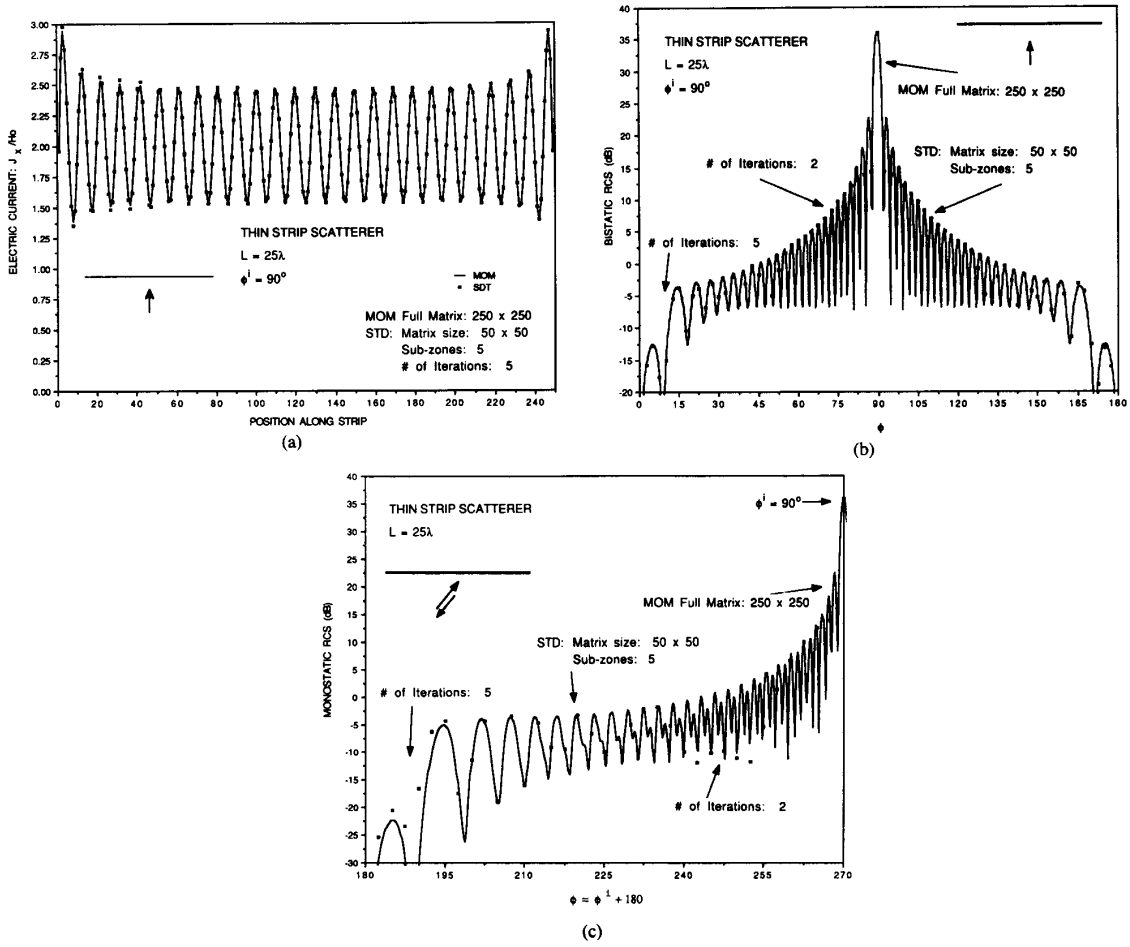

Fig. 6. (a) Distribution of the equivalent electric current on the thin strip scatterer—TE normal excitation. (b) Bistatic radar cross section of the thin strip scatterer—TE normal excitation. (c) Monostatic radar cross section of the thin strip scatterer—TE normal excitation.

(50 × 50) for each subzone modeling. Using the OSRC TE-boundary operator [24], an approximate relationship for the tangential electric current on the perfectly conducting convex scatterer is obtained

$$\hat{s}' J_\tau(\bar{\rho}') = \hat{\nu}' \times \left[\hat{z}' H_z^i(\bar{\rho}') + \hat{z}' H_z^s(\bar{\rho}')\right], \qquad \bar{\rho}' \text{ on } C \tag{14a}$$

$$\frac{\partial H_z^s(\bar{\rho}')}{\partial \nu'} = -\left[\frac{\xi(s')}{2} + jk_1 + \frac{j\xi^2(s')}{8[k_1 - j\xi(s')]}\right] H_z^s(\bar{\rho}') \tag{14b}$$

$$E_\tau^i(\bar{\rho}') = \frac{1}{j\omega\epsilon}\frac{\partial}{\partial \nu'} H_z^s(\bar{\rho}'). \tag{14c}$$

With normal excitation, the above OSRC expression yields an initial current distribution, which is a flat current, with no standing wave distribution along the thin strip scatterer. In fact, the process of the SDT is to sequentially update this initial current for each subzone. In Fig. 6(a) is also shown the magnitude distribution of electric current calculated based on the SDT (with five spatial subzones, $N = 5$). The result shown is obtained for five sweeps with less than 1% error in the region separating adjacent subzones. Fig. 6(b) shows a plot of the bistatic radar cross section obtained using SDT compared with the direct MM solution. In the angular range of $\phi = 30°$ to 150°, the bistatic radar cross section converges in two sweeps with less than 1% error, but for the grazing observation angles more sweeps are required, and for the result shown five sweeps are utilized. Fig. 6(c) shows a plot of the monostatic radar cross section obtained using SDT compared with the direct MM solution.

VI. Homogeneous Dielectric Scatterer—TM Case

Referring to Figs. 2(a) and 2(b), the spatial decomposition technique presented in Section II is now applied for the case of isotropic, homogeneous, lossless dielectric rectangular scatterer of length $L = 10\lambda$ and width $W = 0.25\lambda$ (where λ is the free space wavelength) with TM excitation. The angle of incidence is $\phi^i = 90°$, and the relative permittivity and permeability of the lossless dielectric scatterer are selected as $\epsilon_r = 2.56$ and $\mu_r = 1.0$. Applying the CFIE discussed in Section II and using a full matrix of size (420 × 420), the electric and magnetic current distributions are calculated first, and then the bistatic radar cross section is obtained as shown in Fig. 7. In order to apply the spatial decomposition technique, the dielectric rectangular scatterer is divided into five subzones, $N = 5$, and the SDT matrix size is chosen with same uniform resolution for each subzone modeling. The initial distributions of the axial electric current and tangential magnetic current on the dielectric scatterer are obtained using the first-order OSRC boundary operator [23]. The two current distributions are sequentially updated using the SDT. Fig. 7 also shows a plot of the bistatic radar cross section obtained using SDT compared with the direct MM solution. The bistatic radar cross section converges in one or two sweeps for broad side angles and takes more sweeps for grazing incident angles. The SDT numerical data is obtained with three sweeps with less than 1% error.

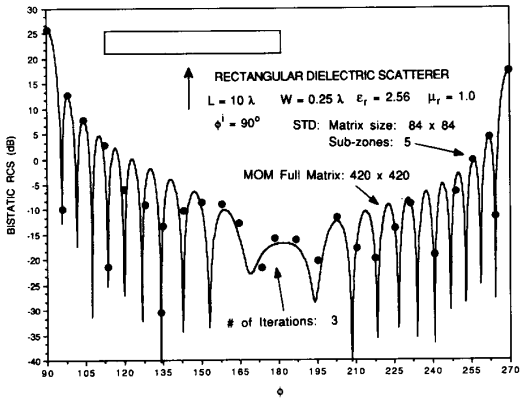

Fig. 7. Bistatic radar cross section of the rectangular dielectric scatterer—TM normal excitation.

TABLE IV
Computer Resources: Direct MM versus SDT

a) Bistatic Radar Cross Section of Thin Strip

Excitation	Strip Size (λ)	Direct MM Matrix Size	MM Run Time (s)	SDT Matrix Size	SDT(*) Run Time (s)
TM	10	200	205	50	34
TM	25	500	3175	50	83
TE	10	200	282	50	45
TE	25	500	4210	50	109

b) Bistatic Radar Cross Section of Wedge with Half-Cylinder

Excitation	Direct MM Matrix Size	MM Run Time (s)	SDT Matrix Size	SDT(*) Run Time (s)
TM	500	4137	100	167
			50	55

VI. Remarks

Using rigorous electromagnetic equivalence, the spatial decomposition technique divides an electrically large object into a multiplicity of subzones. The technique permits limiting the size of the method of moments system matrix that need be inverted regardless of the electrical size of the large scattering object being modeled. Several numerical scattering case studies have also been reported along with comparison and relative error estimation based on condition numbers to expose possible applicability of the spatial decomposition technique to the two-dimensional scattering study of electrically large conducting and dielectric objects. Details of the computational burden to obtain bistatic radar cross section of 1) two thin perfectly

conducting strips of lengths 10 λ and 25 λ and 2) wedge with half-cylinder structure using the direct MM technique and the SDT are reported for the TM and TE excitations.

It can be inferred from Table IV that the spatial decomposition technique can provide order (100:1) savings in computer resources over the direct MM solution for electrically large geometries. This comparative savings appears to increase with the size of the scatterer. In fact, as the MM matrix size increases by a factor of R and the direct MM run time increases by R^3, the SDT run time increases only by R. This may be quite significant.

REFERENCES

[1] A. J. Poggio and E. K. Miller, "Integral equation solutions of three dimensional scattering problems," in *Computer Techniques for Electromagnetics*, R. Mittra, Ed. Elmsford, NY: Pergamon, 1973, ch. IV.

[2] J. R. Mautz and R. F. Harrington, "A combined-source solution for radiation and scattering from a perfectly conducting body," *IEEE Trans. Antennas Propagat.*, vol. AP-27, pp. 445–454, 1979.

[3] K. Umashankar, "Numerical analysis of electromagnetic wave scattering and interaction based on frequency domain integral equation and method of moments techniques," *Wave Motion*, no. 10, pp. 493–525, Dec. 1988.

[4] R. F. Harrington, *Field Computation by Moment Methods*. New York: MacMillan, 1968.

[5] B. J. Strait, Ed., *Applications of the Method of Moments to Electromagnetic Fields*. SCEEE Press, 1981.

[6] A. W. Glisson, "On the development of numerical techniques for treating arbitrary-shaped surfaces," Ph.D. dissertation, Univ. Mississippi, University, MS, 1978.

[7] K. Umashankar and A. Taflove, "Analytical models for electromagnetic scattering," Hanscom Air Force Base, MA, Final Tech. Rep. F19628-82-C-0140, RADC/ESD, June 1984.

[8] S. M. Rao, D. R. Wilton, and A. W. Glisson, "Electromagnetic scattering by surfaces of arbitrary shape," *IEEE Trans. Antennas Propagat.*, vol. AP-30, pp. 409–418, 1982.

[9] K. Umashankar, A. Taflove, and S. M. Rao, "Electromagnetic scattering by arbitrary shaped three dimensional homogeneous lossy dielectric objects," *IEEE Trans. Antennas Propagat.*, vol. AP-34, pp. 758–766, June 1986.

[10] T. K. Sarkar, K. Siarkiewicz, and R. Stratton, "Survey of numerical methods for solution of large systems of linear equations for electromagnetic field problems," *IEEE Trans. Antennas Propagat.*, vol. AP-29, pp. 847–856, 1981.

[11] R. Mittra and C. A. Klein, "Stability and convergence of methods of moments solutions," in *Numerical and Asymptotic Techniques in Electromagnetics*, R. Mittra, Ed. New York: Springer-Verlag, 1975, pp. 129–133.

[12] W. L. Ko and R. Mittra, "A new approach based on combination of integral equation and asymptotic techniques for solving electromagnetic scattering problems," *IEEE Trans. Antennas Propagat.*, vol. AP-25, pp. 187–197, 1977.

[13] W. D. Burnside, C. L. Yu, and R. J. Marhefka, "A technique to combine the geometrical theory of diffraction and the method of moment method," *IEEE Trans. on Antennas Propagat.*, vol. AP-23, pp. 551–557, 1975.

[14] T. J. Kim and G. A. Thiele, "A hybrid diffraction technique—General theory and applications," *IEEE Trans. Antennas Propagat.*, vol. AP-30, pp. 888–897, 1982.

[15] L. N. Medgyesi-Mitschang and D. Wang, "Hybrid solutions for scattering from perfectly conducting bodies of revolution," *IEEE Trans. Antennas Propagat.*, vol. AP-31, pp. 570–583, July 1983.

[16] T. K. Sarkar, X. Yang, and E. Arvas, "A limited survey of various conjugate gradient methods for solving complex matrix equations arising in electromagnetic wave interactions," *Wave Motion*, no. 10, pp. 527–546, Dec. 1988.

[17] R. Mittra and T. S. Li, "A spectral domain approach to the numerical solution of electromagnetic scattering problems," *AEU Electron. and Commun.*, band 29, pp. 217–222, 1975.

[18] K. R. Umashankar, S. Nimmagadda, and A. Taflove, "Application of integral equation and method of moments for electrically very large scatterers using spatial decomposition technique," in *1990 APS / URSI Int. Symp. Dig.*, vol. 1, pp. 76–79, Dallas, TX, May 1990.

[19] K. Umashankar, "Analysis of the electromagnetic scattering by electrically very large objects based on the spatial decomposition technique," Final Tech. Rep., Univ. Illinois, Chicago, Chicago, IL, Jan. 1988.

[20] S. A. Schelkunoff, "Field equivalence theorems," *Comm. Pure Appl. Math.*, vol. 4, pp. 43–59, June 1951.

[21] C. Klein and R. Mittra, "Stability of matrix equations arising in electromagnetics," *IEEE Trans. Antennas Propagat.*, vol. AP-31, pp. 902–905, Nov. 1973.

[22] G. E. Forsythe and C. B. Moler, *Computer Solution of Linear Algebraic Systems*. Englewood Cliffs, NJ: Prentice-Hall, 1967.

[23] R. G. Kouyoumijan and P. H. Pathak, "A uniform geometrical theory of diffraction of an edge in a perfectly conducting surface," *Proc. IEEE*, vol. 62, pp. 1448–1461, Nov. 1974.

[24] G. A. Kriegsmann, A. Taflove, and K. Umashankar, "A new formulation of electromagnetic wave scattering using an on-surface radiation boundary condition," *IEEE Trans. Antennas Propagat.*, vol. AP-35, pp. 153–161, 1987.

[25] S. Arendt, K. Umashankar, A. Taflove and G. A. Kriegsmann, "Extension of on-surface radiation condition theory to scattering by two-dimensional homogeneous dielectric objects," *IEEE Trans. Antennas Propagat.*, vol. 38, pp. 387–406, Dec. 1990.

[26] K. R. Umashankar, S. Nimmagadda, and A. Taflove, "Numerical analysis of electromagnetic scattering by electrically large objects using spatial decomposition technique," in *1991 Progress in Electromagn. Res. Symp. Proc.*, Cambridge, MA, July 1991.

Korada R. Umashankar (S'69–M'75–SM'81), for a photograph and biography please see page 1212 of the August 1991 issue of this TRANSACTIONS.

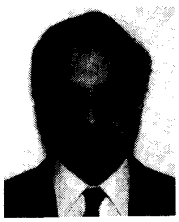

Sainath Nimmagadda (S'89) was born in Kurnool, India. He received the B.S.E.E. degree from Jawaharlal Nehru Technological University, India, in 1979 and the M.S.E.E. degree from the Indian Institute of Technology, Kharagpur, India, in 1981. He is currently working toward the Ph.D. degree at the University of Illinois, Chicago.

During 1981–1988, he was an Assistant Professor at Bangalore University and Osmania University. Since 1988, he has been working as a Research Assistant in the Department of Electrical Engineering and Computer Science. His present research interests include numerical methods for electromagnetic field scattering and interaction, simulation of high-frequency, high-speed compound semiconductor devices, supercomputing of electromagnetic phenomena and 3-D visualization of transient fields.

Allen Taflove (M'75–SM'84–F'90), for a photograph and biography please see page 906 of the July 1991 issue of this TRANSACTIONS.